Sensors and Materials, Vol. 29, No. 4 (2017) 497–509
MYU Tokyo

S & M 1343

Development of Piezoelectric Fibers in Smart Patch by Near-Field Electrospinning Method with Closed-Loop Motor Control

Cheng-Tang Pan,[1,2] Kuo-Chang Tsai,[1*] Shao-Yu Wang,[1]
Chung-Kun Yen,[1] Yun-Ping Sun,[3] and Chih-Hao Tsao[1]

[1]Department of Mechanical and Electro-Mechanical Engineering, National Sun Yat-sen University,
No. 70, Lien-hai Rd., Kaohsiung 80424, Taiwan
[2]Institute of Medical Science and Technology, National Sun Yat-sen University,
No. 70, Lien-hai Rd., Kaohsiung 80424, Taiwan
[3]Department of Mechanical Engineering, Cheng Shiu University,
No. 840, Chengcing Rd., Niaosong Dist., Kaohsiung 83347, Taiwan

(Received September 30, 2016; accepted January 19, 2017)

Keywords: closed-loop control, PVDF, piezoelectric fibers, near-field electrospinning, smart patch

In this report, we present a closed-loop motor control for a cylindrical collector to obtain continuous and uniform polyvinylidene fluoride (PVDF) piezoelectric nanofibers using near-field electrospinning (NFES) to fabricate PVDF fibers with piezoelectric properties. The fibers were applied to make a force sensor packaged in a smart patch. The analysis of the PVDF process includes determination of concentration, viscosity, electrical conductance, and contact angle. The optimal parameters were determined to make continuous PVDF fibers. The fibers were packaged in polydimethylsiloxane (PDMS) with interdigitated electrode (IED) structures. The molds of IED 1 mm thick with a 0.2 to 1 mm pitch were fabricated by electrical discharge machining (EDM). A conductive silver gel was coated on the IED by soft contact lithography. The fibers on the IED were repolarized at temperature of 65 °C and an electrical field of 7 V/μm. This patch was measured with a voltage signal from 42 to 280 mV under beating forces of 0.05 to 0.5 N. In addition, the average voltage was 104 mV when the work temperature was 25 to 100 °C.

1. Introduction

Fiber-based piezoelectric sensors can be applied to various sensing systems such as those for force and strain. Polyvinylidene fluoride (PVDF) has potential for use as a piezoelectric polymer because of its high flexibility, biocompatibility, and low cost. These features make PVDF attractive for transducer applications including microelectric-mechanical devices, electromechanical actuators, and force sensors. PVDF is a semicrystalline polymer consisting of four crystalline phases (α, β, γ, and δ).[1–3] PVDF with a nonpolar α phase is most commonly found in commercially available films. Since the dipole moments in this phase have a random orientation, they cancel each other out. The β phase has dipole moments pointing in the same direction; the β phase is responsible for the piezoelectric properties of the PVDF polymer.[4–7] Many studies focused on the far-field electrospinning (FFES) technique[8,9] and near-field electrospinning (NFES) technology[10,11]

*Corresponding author: e-mail: vongohking@yahoo.com.tw
http://dx.doi.org/10.18494/SAM.2017.1532

ISSN 0914-4935

to improve the piezoelectric properties. Electrospinning was first patented in the US in 1902. This process was largely forgotten until the 1990s.[13,14] With the improvement and rapid development of nanofiber applications, electrospinning has become useful in this field.[15] Electrospinning is currently a technique that allows the fabrication of continuous fibers with diameters down to a few micrometers. The diameter and morphology of electrospun fibers can be controlled by adjusting the parameters of molecular weight, solution properties (viscosity, conductivity, and surface tension), electrical potential, flow rate, and distance (between the needle and collector) during electrospinning.[16]

In this study, we focused on NFES with a closed-loop control motor to fabricate PVDF fibers with piezoelectric properties. A cylindrical collector was used to collect continuous fibers and fabrics. Then, the fibers were tailored to make a force sensor array attached to a smart patch. In the process, the analysis determines concentration, viscosity, electrical conductance, and contact angle. The fibers were packaged in polydimethylsiloxane (PDMS) with interdigitated electrodes (IDEs) and embedded in a smart patch. The IDE mold was fabricated by electrical discharge machining (EDM). Finally, this smart patch was applied to detect the force and temperature immediately for paralyzed patients.

2. Experimental Method

In this study, the NFES combined with a rolling collection device was used to fabricate orderly piezoelectric PVDF fibers. The optimal parameters for the fabrication of the PVDF fibers were determined in terms of concentration, viscosity, electrical conductance, and contact angle of PVDF solution. Scanning electron microscopy (SEM) was used to analyze the morphology of the fibers. Finally, a high-voltage electrical field was used to repolarize the PVDF using the IDE. This smart patch can be applied to detect the temperature and force over a large area immediately.

2.1 PVDF solution

For the PVDF solution, dimethyl sulfoxide (DMSO) was used as the solvent to dissolve PVDF powder (Mw = 534000). A fluorosurfactant (ZONYL® UR) and acetone were used to reduce the surface tension and improve the evaporation rate of the PVDF solution, respectively. During the NFES process, an electrical field was applied to the solution to make the droplets of the solution break through the surface tension and form a Taylor cone. Increasing the charges on the droplets was an easier way to form a Taylor cone. In addition, different concentrations of solutions possessed different conductivities. When the concentration of the solution was too high, discontinuous droplets formed. A low viscosity of the solution because of a low concentration could lead to the formation of excessively large droplets, which could drop on the collecting device and cause a short circuit. Table 1 shows the concentration ratio, which was investigated to obtain the optimal parameters for the electrospinning process.

2.2 NFES process and rolling collection device with closed-loop control

The PVDF solution was filled into a syringe that was connected to an infusion pump. The stainless needle of the syringe was connected to a high-voltage supply to form a high electrical field during the NFES process. A rolling collector was grounded and connected with the motor of a closed-loop control. An X–Y two-axis digital control platform was used to control the electrospun

Table 1
Content of PVDF solution for various concentration ratios.

PVDF solution (PVDF/solvent)	PVDF powder (g)	Solvent (g)		Surfactant (g)
		DMSO	Acetone	
15 wt%	0.75	2.5	2.5	0.2
16 wt%	0.8	2.5	2.5	0.2
17 wt%	0.85	2.5	2.5	0.2
18 wt%	0.9	2.5	2.5	0.2
19 wt%	0.95	2.5	2.5	0.2

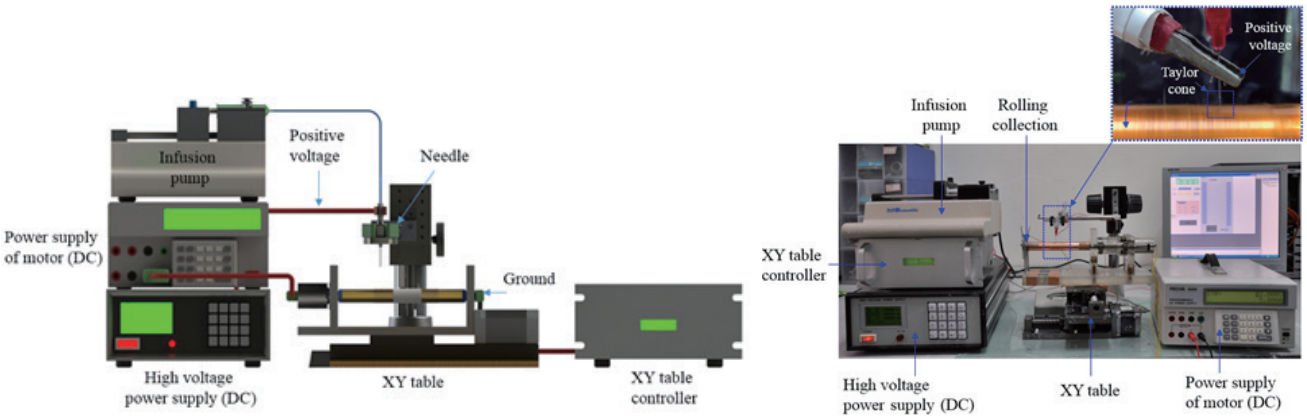

Fig. 1. (Color online) Experimental setup of NFES: (a) schematic diagram and (b) detailed setup.

piezoelectric fibers. Figure 1(a) shows a schematic diagram of the NFES configuration. The solution electrospun out of the tip of the needle is affected by the electrical field. The positive ions accumulate on the droplet surface because of the repelling force. When the repelling force is larger than the surface tension, the tip of hemispherical droplet forms a Taylor cone. Then, the fibers are spun along the direction of the applied electrical field. Because of the high electrical field and the specific direction of collection, a directional dipole moment in the materials could be obtained. The experimental setup of NFES includes a needle clamping apparatus, an infusion pump, a high voltage-power supply, a rolling collection device mounted on a motor, and a *X*–*Y* motion stage (controlled by an *X*–*Y* stage controller via computer). High voltage from 10 to 16 kV was applied to produce a high electrical field (1×10^7–1.6×10^7 V/m) between the needle and the collector (the gap between the needle and the collector is set as 1–2 mm), as shown in Fig. 1(b). This experimental device was built with the motor of AKD Servo Drives (National Instruments AKD-P00306) and the Brushless Servo Motors (National Instruments AKM11B), which were utilized to operate the closed-loop motor control. The AKD WorkBench human–machine interface (HMI) software was designed by Kollmorgen, a provider of components and motion systems. The HMI software allowed us to tune the parameters of the AKD servo motor easily. A standard Ethernet for Control Automation Technology (EtherCAT) was connected to the drive to change and to view the driving parameters in the AKD WorkBench quickly and easily. The whole system configuration of the closed-loop motor control is shown in Fig. 2. By means of fast control-loop updating rates, the closed-loop motor control can guarantee a reliable control performance and can accommodate the changing load conditions.

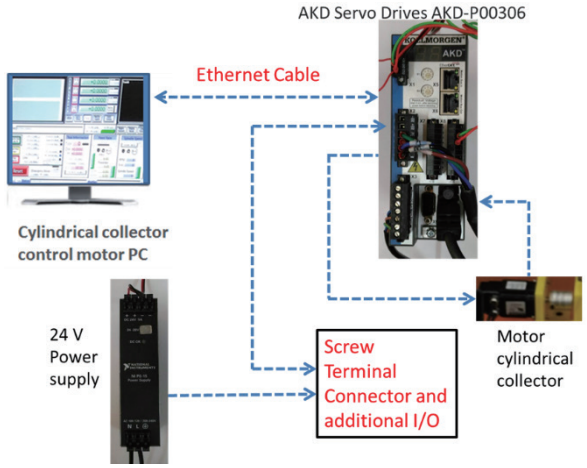

Fig. 2. (Color online) Configuration of the closed-loop motor control system.

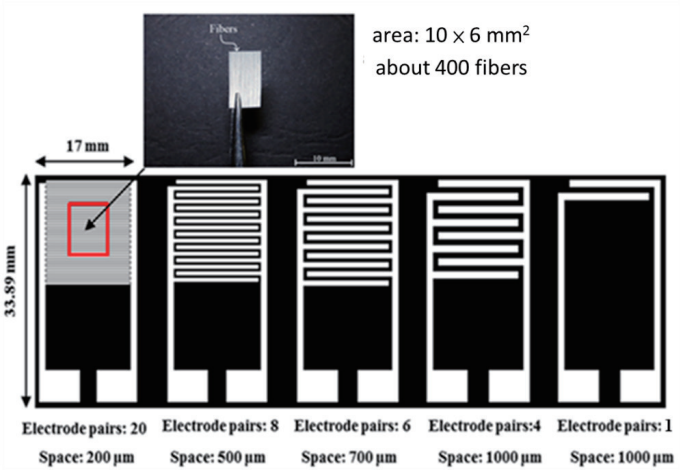

Fig. 3. (Color online) Design of IDE.

2.3 Repolarization process and measurement of piezoelectric fibers

Figure 3 shows the PVDF piezoelectric fibers (area: 10 × 6 mm², about 400 fibers) that were laid on various flexible IDEs. Through the repolarization process with 1400 to 7000 V at 65 °C for 1 h, as listed in Table 2, the fibers generated a regional dipole moment corresponding to the electrode pairs. For the measurement process, compression and tension were exerted on the piezoelectric fibers to obtain the potential voltage. Figure 4 shows a photo of the measurement system. A rotating rod connecting to a rotary motor was used to produce low-frequency vibration at the free end of the PDMS with embedded fibers and to produce axial strain in the fibers. An infrared tachometer was adopted to measure the rotational speed of the motor and convert it into frequency. A power supply was used to drive the motor and control angular speed. Finally, the induced electric potential and current signals generated from the test samples were measured using voltage and current meters. A strain gauge was applied to measure the strain on electrospun fibers. The test samples were characterized under repeated external strains by controlling the deformation magnitude of the vibration. The bending force resulted in mechanical strain, which distributed along the fibers and then converted to alternating voltage and current through the piezoelectric d_{33} mode.

2.4 Fabrication and measurements with the PDMS smart patch

PDMS was used as packaging material because PDMS can be easily molded. In the experiment, the mold with IDE patterns was made with an EDM (CREATOR CR-5). Then, the PDMS was molded. The electromechanical conversion efficiency and sensing area can be enhanced through repolarization using the IDE. Conductive silver gel was printed on the surface by soft contact lithography. Figure 5(a) shows the stainless steel mold made by EDM. Then, with this mold, the PDMS was molded, as shown in Fig. 5(b). After the demolding process, the PDMS was coated with a layer of silver gel by soft contact lithography, as shown in Fig. 5(c). Then, fibers were laid atop the silver gel electrodes. Finally, PDMS was cast atop the fibers as a protective layer, as

Table 2
Repolarization parameters of interdigitated electrode.

Voltage (V)	Temperature (°C)	Time (h)
1400	65	1
3500	65	1
4900	65	1
7000	65	1

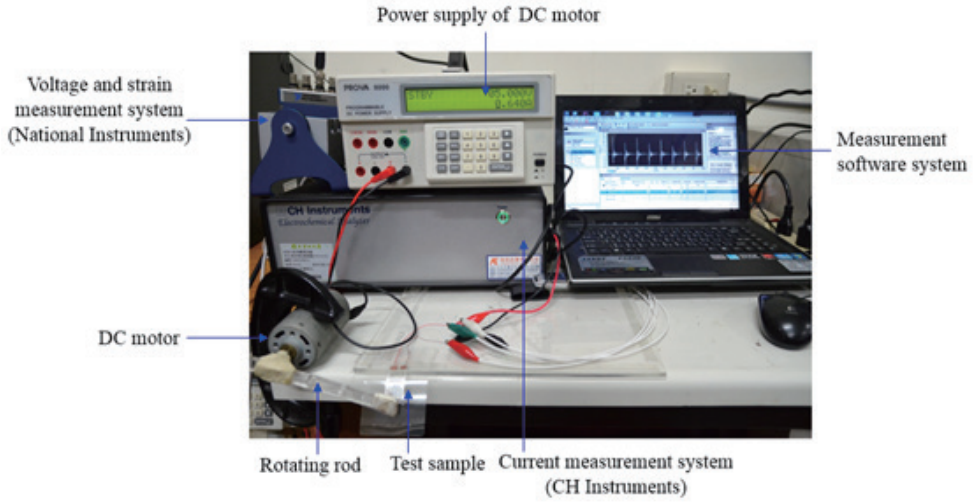

Fig. 4. (Color online) Measurement system for vibration.

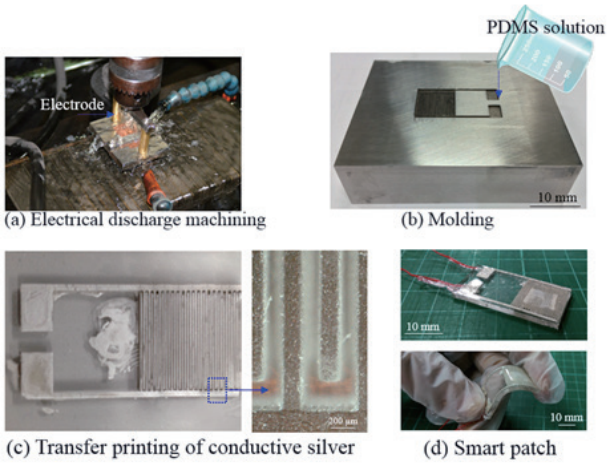

Fig. 5. (Color online) Fabrication sequence of PDMS-based smart patch.

shown in Fig. 5(d). For the measurement of the PDMS-based smart patch, the reliability test was carried out by beating the patch at 2 to 8 Hz. The voltage output was measured. Finally, through the array arrangement inside the smart patch with a temperature-sensing device, the smart patch could immediately detect the temperature and force over a large area.

3. Results and Discussion

3.1 Relationship between PVDF solution parameters and NFES process with closed-loop control

The characteristics of the PVDF solution include concentration, viscosity, electrical conductance, and contact angle. Figure 6 shows the measured conductivity of PVDF solutions with different concentrations. In the study, we investigated conductivities of 15 to 19 wt% concentrations of the PVDF solutions. Then, the PDMS solution with the highest conductivity was chosen for the NFES. The result shows that the 18 wt% PVDF solution possessed the highest conductivity of 43.9 μS/cm. That means that the 18 wt% PVDF solution can easily accumulate charge in droplets and made them break through the surface tension and form fibers. Figures 7(a) and 7(b) show the viscosity values from 716.8 to 657.9 cP and the 31.25° contact angle, respectively. The solution was sticky and hydrophilic and needed a higher electrical field to spin out the fibers.

The concentrations of the PVDF solutions was examined from 15 to 18 wt%. The relationship between the solution concentration and fiber diameters is shown in Fig. 8, which also reveals the relationship between the morphology and the diameters of the fibers observed by SEM. The diameter ranged from 0.5 to 4 μm. The smallest diameter fiber of 0.97 μm can be obtained when

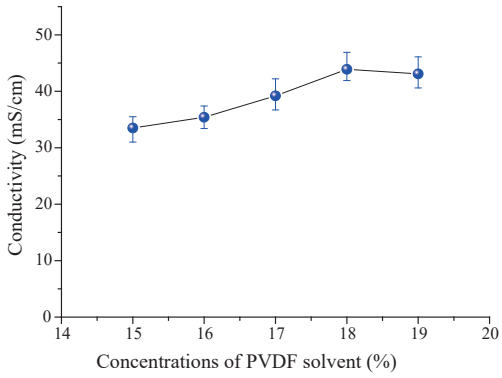

Fig. 6. (Color online) Different concentrations of PVDF solution in electrical conductance measurement.

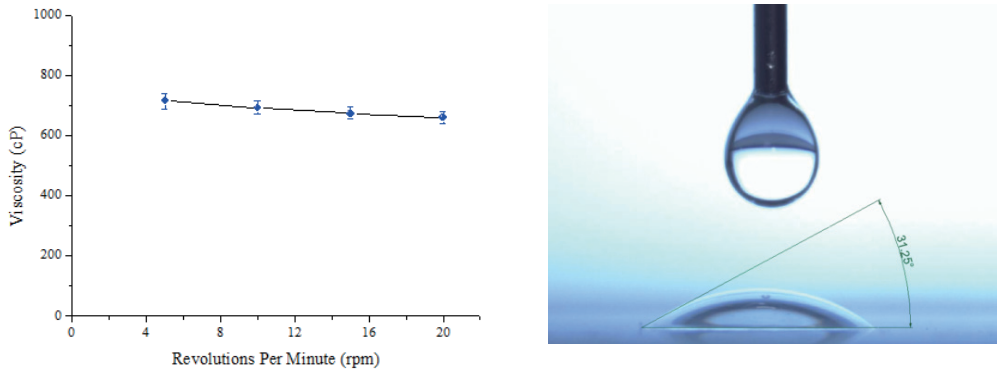

(a) (b)

Fig. 7. (Color online) (a) Viscosity and (b) contact angle of 18 wt% PVDF solution.

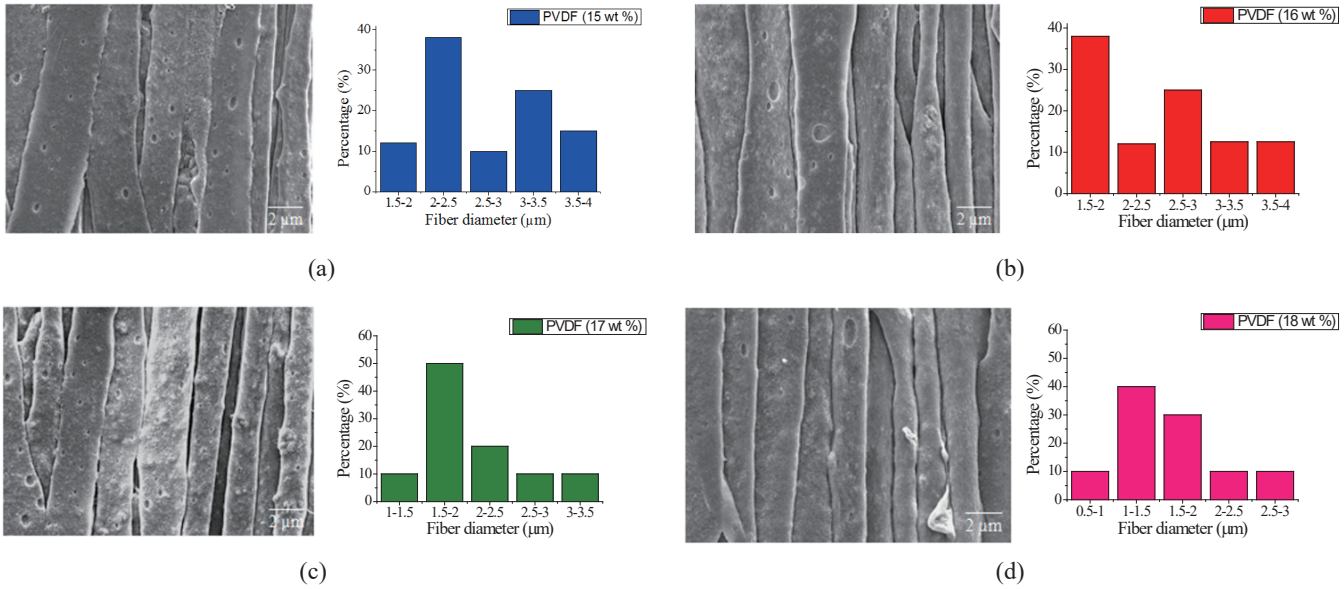

Fig. 8. (Color online) Relationship of solution concentration and fiber diameters under 1.6×10^7 V/m electric field, 0.01 ml/min flow rate, 0.381 mm inner diameter of the needle: PVDF solutions of concentrations of (a) 15, (b) 16, (c) 17, and (d) 18 wt%.

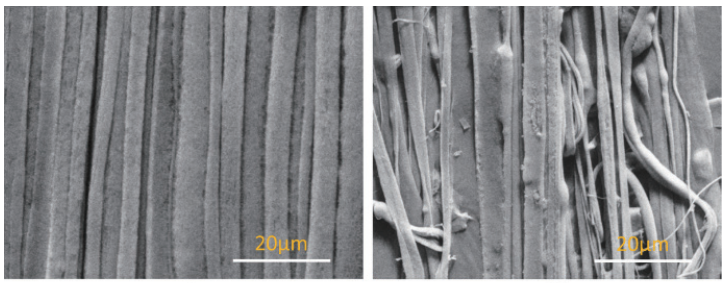

Fig. 9. (Color online) SEM images of PVDF fibers fabricated with (a) closed-loop motor control system and (b) open-loop system.

the 18 wt% solution was used. The diameter of PVDF piezoelectric fibers gradually decreased as the concentration increased.

PVDF fibers fabricated with the closed-loop motor control system and the open-loop system were observed by SEM, as shown in Figs. 9(a) and 9(b). By comparing Figs. 9(a) and 9(b), we can easily see that the closed-loop motor control fibers having uniform spacing distances and diameters. The closed-loop motor control system was able to achieve the uniform spacing distances owing to its stable cylindrical collector speed. The stable cylindrical collector speed achieved uniform spacing distances, while the fluctuating cylindrical collector speed led to various spacing distances.

Figure 10 shows the graphs of cylindrical collector speeds at 900, 1500, and 1900 rpm from the closed-loop motor control system and open-loop system. In closed-loop motor control system, the speed of cylindrical collector was able to be maintained with desired speed commands during the NFES operation, but in open-loop system, the speed fluctuated during NFES operation. Thus,

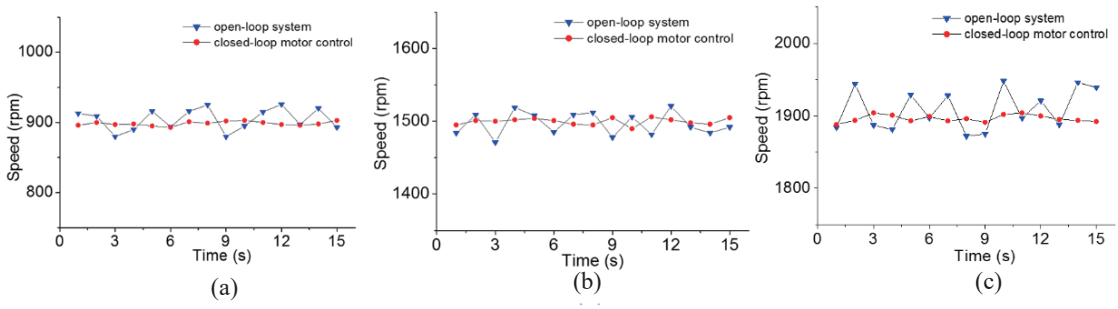

Fig. 10. (Color online) Cylindrical collector speeds of (a) 900, (b) 1500, and (c) 1900 rpm with closed-loop motor control system and open-loop control system.

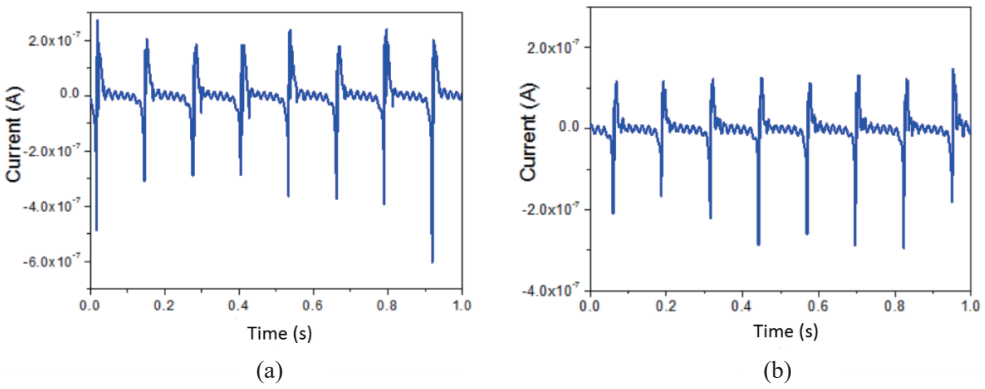

Fig. 11. (Color online) (a) Closed-loop motor control current and (b) open-loop current.

the closed-loop motor control system had greater accuracy than the open-loop system. Therefore, a collector with constant force achieved uniform diameters, whereas an unstable force resulted in varying diameters.

Figure 11 shows current plots from the tapping test: Fig. 11(a) using the closed-loop motor control system and 11(b) using the open-loop system. After the tapping test with the closed-loop motor control system, we achieved a positive average current of about 2.1×10^{-7} A and a negative average current of about -3.4×10^{-7} A. In comparison with the positive average current of about 1.3×10^{-7} A and the negative average current of about -2.5×10^{-7} A of the open-loop system, the closed-loop control achieved a good improvement. Thus, a clear advantage can be found in the closed-loop motor control system over the open-loop system: higher currents [$(2.1 \times 10^{-7} > 1.3 \times 10^{-7}$; $3.4 \times 10^{-7} > 2.5 \times 10^{-7}$ (a negative value means the opposite direction, so it can be neglected)].

Figure 12 shows plots of voltage in the tapping test: Fig. 12(a) using the closed-loop motor control system and 12(b) using the open-loop system. After the tapping test with the closed-loop motor control system, we achieved a positive average voltage of about 0.08 V and a negative average voltage of about −0.12 V. In comparison with positive average current of about 0.07 V and negative average current of about −0.06 V in the open-loop system, the closed-loop motor control system also achieved a good improvement. Thus, a clear advantage can be found in the closed-loop motor control system over the open-loop system: higher voltages [(0.08 > 0.07; 0.12 > 0.06 (a negative value means the opposite direction, so it can be neglected)]. The improvement was easily seen, even though the improvement was not as large as in the current case.

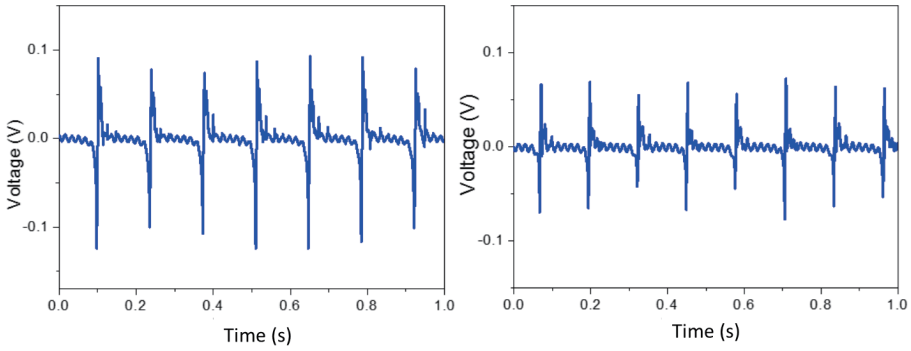

(a) (b)

Fig. 12. (Color online) (a) Closed-loop motor control voltage and (b) open-loop voltage.

To confirm that the signals came from the piezoelectric property, we carried out another voltage measurement with the reverse electric connection for confirmation. These reverse voltage signals of PVDF fibers were attained using a tapping frequency at 5 Hz. A comparison of the forward electric connection graph [as shown in Fig. 13(a)] with the reverse connection graph [as shown in Fig. 13(b)] of the closed-loop motor control system shows that the pattern of data for the reverse connection is "upside down" because of the reverse connecting. The result shows evidence that the signals came from the piezoelectric property of PVDF fibers. In the open-loop system, the forward connection and reverse connection are shown in Figs. 13 (c) and 13(d). The graph of the open-loop control case also has an "upside down" pattern.

3.2 Properties and characteristics of PVDF fiber

Figure 14(a) demonstrates that the diameters of the PVDF fibers shrank from 33.4 to 13.1 μm in the closed-loop motor control system and shrank from 33.6 to 14.0 μm in the open-loop system with an increase of the tangential velocity of the cylindrical collector from 943 to 1990 mm/s. At a higher tangential velocity of the cylindrical collector, the PVDF fibers bore a greater pulling force which led to the production of fibers with smaller diameters. Figure 14(b) shows the diameters of the PVDF fibers in different electrical fields (E = 1.3 × 10^7, 1.5 × 10^7, and 1.7 × 10^7 V/m,). Higher electrostatic fields led to larger electrostatic forces and resulted in thinner PVDF fibers. The diameter of the PVDF fibers shrank from 24.1 to 15.3 μm in the closed-loop motor control system (with less fluctuation) and shrank from 25.1 to 16.5 μm in the open-loop system (with greater fluctuation) when the electrical field increased from 1.3 × 10^7 to 1.7 × 10^7 V/m. These diameters shrank on increasing the electrical field, but short-circuiting could occur when the electrical field was too high. Consequently, the electricspinning field had to be controlled within a suitable voltage range.

3.3 PVDF piezoelectric fibers with repolarization treatment

The effect of the IDE pitch on voltage and current output is discussed in this section. Repolarization was applied to change the direction of polarity of each fiber and make each fiber an individual sensing device. Figure 15 shows the schematic of the IDE upon which each fiber can change its dipole direction. The applied repolarizing voltage must be slowly increased to reach an

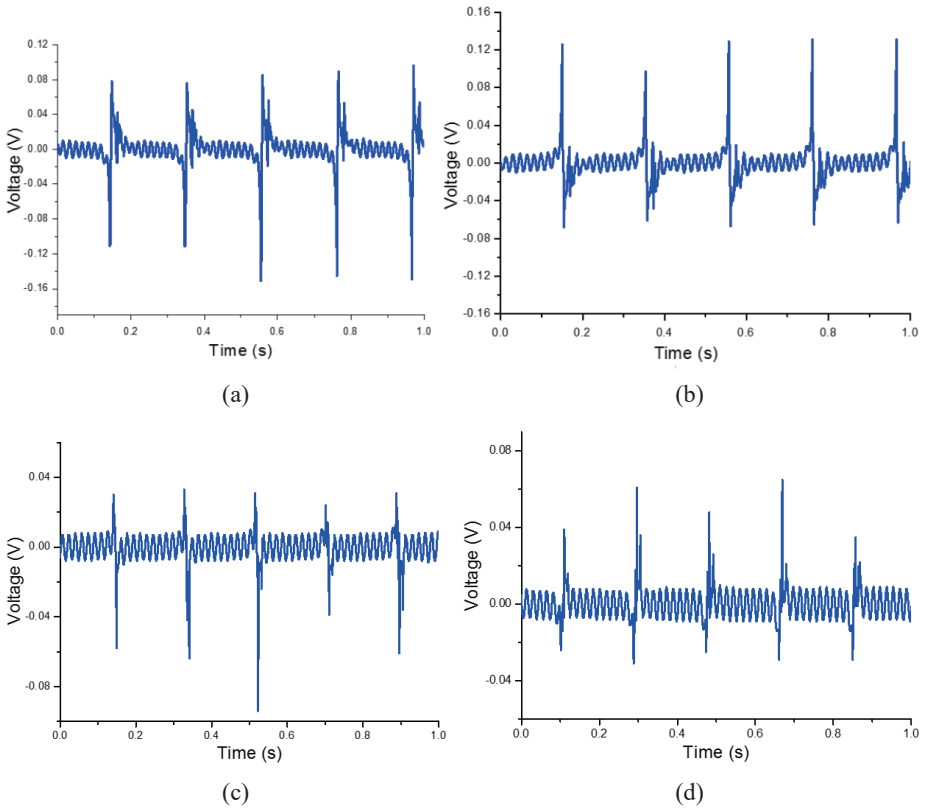

Fig. 13. (Color online) Voltage charts of (a) forward electric connection and (b) reverse connection of closed-loop motor control system. Voltage charts of (c) forward connection and (d) reverse connection of open-loop system.

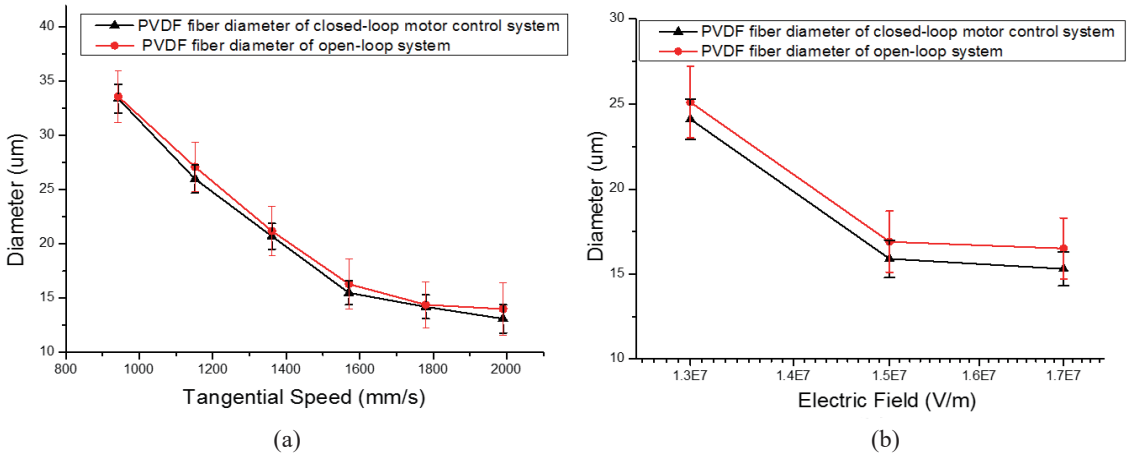

Fig. 14. (Color online) Diameters of PVDF fibers plotted with respect to (a) tangential speed of cylindrical collector and (b) electrical field.

electrical field of 7 V/μm required for polarization. The IDE with 0.2 and 1 mm pitch was studied in this work. Figures 16(a) and 16(b) show the voltage and current output when the fibers were subjected to a strain rate of 0.081 1/s at a frequency of 8 Hz with a rotating beater. When the pitch was 1 mm, the maximum average voltage and current output without repolarization were 36.59 mV

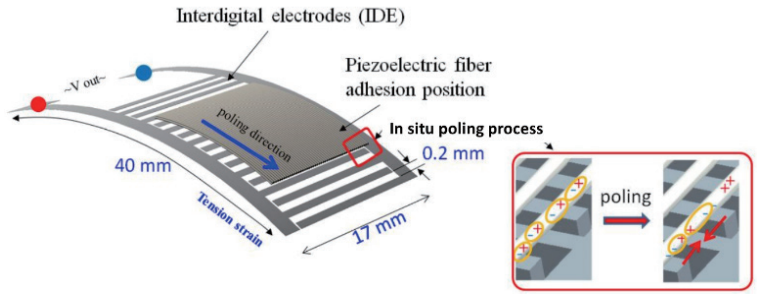

Fig. 15. (Color online) Interdigitated electrode model by which each fiber collects the generated charge to achieve the additive effect.

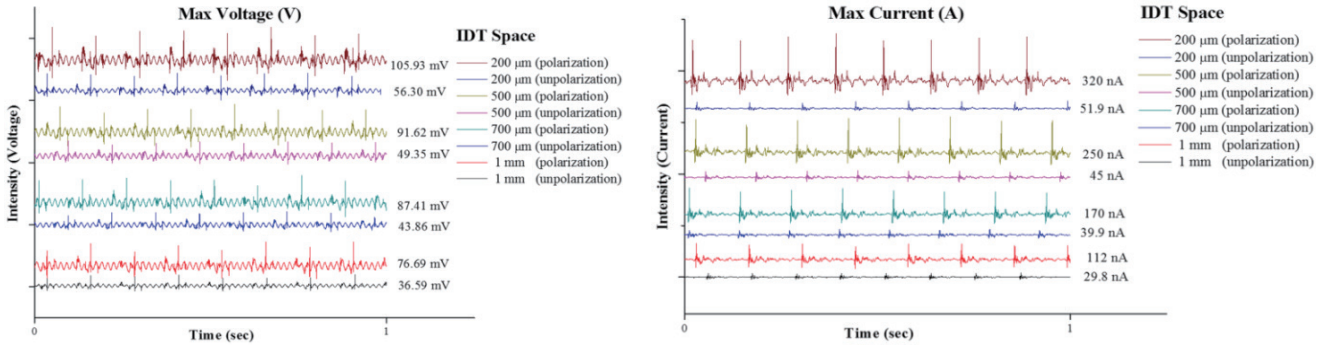

(a) (b)

Fig. 16. (Color online) (a) Voltage and (b) current output when the fibers were subjected to a strain of 0.081 1/s.

and 29.8 nA. After repolarization, the maximum average voltage output and current were 76.69 mV and 112 nA. In addition, when the pitch was decreased to 200 μm, the maximum average voltage and the current output without repolarization were 56.3 mV and 51.9 nA. After repolarization, the maximum average voltage and current output were 105.93 mV and 320 nA. Figure 17 shows that the smart patch senses a voltage output from 42 to 138 mV when small beating forces were exerted on the patch from 0.05 to 0.5 N.

3.4 Electric reliability of PVDF piezoelectric fibers

The electrical property and reliability analysis of the PDMS smart patch is discussed in three ways. First, the maximum and minimum voltages of the PDMS smart patch were measured for beating at different frequencies. Figure 18(a) shows the output voltages as a function of different beating frequencies. The voltages were measured from 0.037 and 0.182 V when the frequencies were 2 and 11 Hz, respectively. However, when the frequency was up to 12 Hz, the voltage decreased to 0.171 V. Since the vibration frequency was higher than the voltage output response, it caused offset phenomenon.

Second, the PDMS smart patch was used to test the temperature effect on the voltage output of PVDF sensors. After heating the smart patch with a PVDF sensor array for 30 min, the voltage variation was analyzed. Figure 18(b) shows that the voltage was 0.116 V when the heating

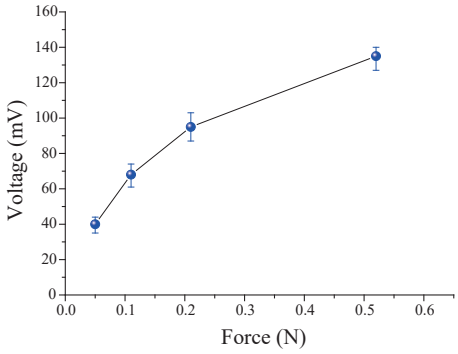

Fig. 17. (Color online) Relationship between voltage output and force for a smart patch.

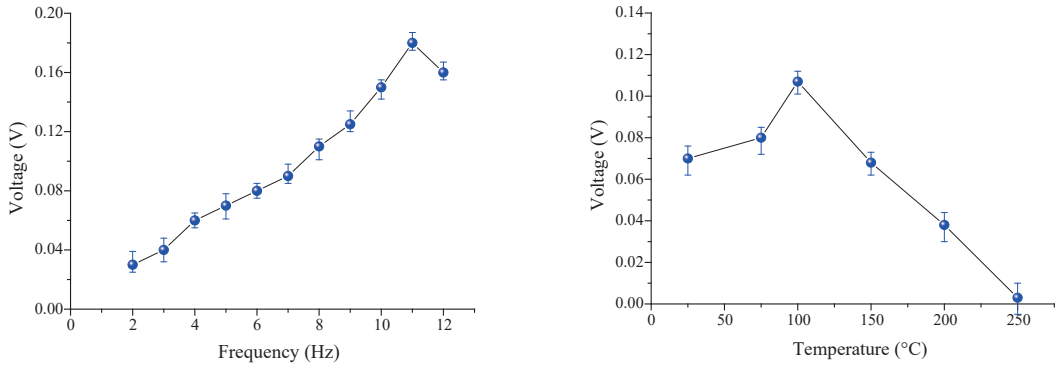

(a) (b)

Fig. 18. (Color online) Reliability analysis of PDMS smart patch: (a) experiment with different beating frequencies and (b) temperature test.

temperature was 100 °C. After that, the voltage decreased gradually. Therefore, it is recommended that the temperature should be below 100 °C.

Third, the patch was subjected to a reliability test. If the PDMS smart patch was shaken by an oscillator from 10 to 40 Hz for 24 h, the PVDF sensor could be damaged. The measurement method was the same as that in the second part of process with a fixed frequency of 2 Hz. The voltage of the smart patch was measured with a NI9234 reader. The experimental result shows that the average voltage was 0.104 V with small deviations, which indicates that the PDMS smart patch possessed good repeatability and reliability.

4. Conclusions

In this study, we present NFES with a closed-loop motor control to fabricate PVDF fibers with piezoelectric properties using a rolling cylindrical collector and demonstrate the clear improvement for a closed-loop motor control system compared with an open-loop system. The fibers and fabric were cut to make a force sensor and a smart patch was installed inside. The relationship between the different concentrations of the PVDF solution and the diameter of the fibers shows that the diameter ranged from 0.5 to 4 μm. The diameter of the PVDF piezoelectric fiber gradually decreased when the concentration was increased. The fiber with the smallest diameter of 0.9–1 μm could be

obtained by using a solution of 18 wt%, when an IDE with a smaller pitch was used, and more IDE electrode pairs were made from the same area after the repolarizing process. The fibers on the IED were repolarized at a temperature of 65 °C and an electrical field of 7 V/μm. This patch can sense a voltage signal from 42 to 280 mV when small beating forces were exerted on the patch from 0.05 to 0.5 N. In addition, the average voltage was 104 mV when the work temperature was 25 to 100 °C. The result shows that the PDMS-based smart patch possessed good repeatability and reliability. In addition, when the pitch was decreased to 200 μm, the maximum average voltage and the current output without repolarization were 56.3 mV and 51.9 nA. After repolarization, the maximum average voltage and current output were 105.93 mV and 320 nA.

Acknowledgements

The authors thank the Ministry of Science and Technology, ROC, for its financial support under grant 103-2221-E-110-009-MY3. We also sincerely thank the National Science Council Core Facilities Laboratory for Nano-Science and Nano-Technology in National Sun Yat-Sen University, Kaohsiung-Pingtung area, Taiwan for support.

References

1 J. M. Ha, H. O. Lim, and N. J. Jo: Adv. Mater. Res. **29** (2007) 363.
2 Z. H. Liu, C. T. Pan, L. W. Lin, and H. W. Lai: Sens. Actuators, A **193** (2013) 13.
3 I. S. Elashmawi, E. M. Abdelrazek, H. M. Ragab, and N. A. Hakeem: Physica B **405** (2010) 94.
4 M. Neidhofer, F. Beaume, L. Ibos, A. Bernes, and C. Lacabanne: Polymer **45** (2004) 1679.
5 Y. Peng and P. Wu: Polymer **45** (2004) 5295.
6 P. Sajkiewicz, A. Wasiak, and Z. Goclowski: Eur. Polym. J. **35** (1999) 423.
7 Y. Chen and C.Y. Shew: Chem. Phys. Lett. **378** (2003) 142.
8 Z. Zhao, J. Li, X. Yuan, X. Li, Y. Zhang, and J. Sheng: J. Appl. Polym. Sci. **97** (2005) 466.
9 X. Ren and Y. Dzenis: Mater. Res. Soc. Symp. Proc. **920** (2006) p. 55.
10 C. Chang, Y. K. Fuh, and L. W. Lin: Solid-State Sensors, Actuators and Microsystems Conf. (2009) p. 1485.
11 D. Sun, C. Chang, S. Li, and L. W. Lin: Nano Lett. **6** (2006) 839.
12 D. Li and Y. Xia: Adv. Mater. **16** (2004) 1151.
13 W. E. Teo and S. Ramakrishna: Nanotechnology **17** (2006) 89.
14 R. Khajavi and M. Abbasipour: Scientia Iranica, Transactions F: Nanotechnology **19** (2012) 2029.
15 R. Dersch, M. Graeser, A. Greiner, and J. H. Wendorff: Aust. J. Chem. **60** (2007) 719.
16 Z.-M. Huang, Y. Z. Zhang, M. Kotaki, and S. Ramakrishna: Comp. Sci. Technol. **63** (2003) 2223.